Supporting Information 1 (SI.1)

Description of the Surface Chemistry, Geometry and Arrangement of the Nanostructures

Table S1a. Symbols used to describe the surface chemistry, geometry and arrangement of the nanostructures.

θ_{ps}	Water contact angle on a flat polystyrene (PS) substrate.
θ_{mtl}	Water contact angle on a flat deposited metal substrate.
X-axis	Axis parallel to the long side of fins and grooves.
Y-axis	Axis parallel to the short side of fins and grooves.
p	Length of the long side of a nanostructure.
q	Spacing between nanostructure tips along the X-axis.
w	Length of the short side of a nanostructure.
v	Spacing between nanostructure tips along the Y-axis.
h	Height of the nanostructures.
δ	Angle of metal evaporation relative to the substrate surface normal.
β	The bearing of the metal deposition direction (in the X-Y plane) with respect to +Y.
α	Angle the sidewall of a nanostructure makes with the horizontal base. This is dependent on the anisotropy of the plasma etching process.

Table S1b. Processing and geometric parameters for freshly fabricated samples. The last column shows schematic diagrams of corresponding nanostructures (Yellow: Metal coated regions White/Gray: Uncoated regions). The arrows next to them indicate the directions of wetting due to anisotropic surface energies of the nanostructures (wetting directions due to topography not included). Measurements of *p*, *q*, *w* and *v* are taken at the tips of the nanostructures.

Sample	Type	h_0 (μm)	p (μm)	q (μm)	w (μm)	v (μm)	α (°)	δ (°)	θ_{mtl} (°)	β (°)	Schematic Diagram
A	Hydrophilic Groove	0.90	-	-	0.13	0.52	75	27	22.2	180	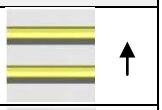
B	Hydrophobic Groove	0.40	-	-	0.08	0.57	85	27	22.2	180	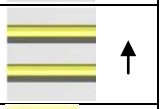
C	Hydrophilic Pillar	1.14	0.05	0.58	0.05	0.58	75	27	22.2	180	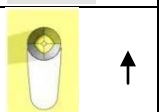
D	Hydrophobic Pillar	1.30	0.12	0.51	0.12	0.51	85	27	22.2	180	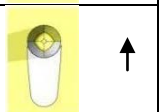
E	Hydrophobic Pillar	1.20	0.20	0.43	0.20	0.43	85	27	22.2	207	
F	Hydrophobic Pillar	1.30	0.12	0.51	0.12	0.51	85	27	22.2	225	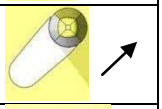
G	Hydrophilic Fin	0.40	1.70	2.76	0.12	0.51	75	27	22.2	180	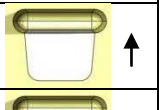
H	Hydrophobic Fin	1.10	3.33	3.93	0.10	0.55	85	27	22.2	180	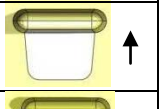
I	Hydrophobic Fin	0.85	1.60	2.80	0.20	0.48	85	27	22.2	210	
J	Hydrophobic Fin	0.60	1.80	2.80	0.15	0.48	85	60	22.2	270	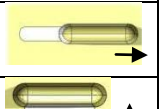
K	Hydrophobic Fin	0.50	2	3.10	0.15	0.49	85	27	24.3	180	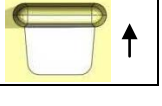

Notes: θ_{ps} was found to be stable for more than the one week period during which all experiments were carried out. Wetting along an axis with anisotropic surface energy always occurs preferentially in the direction of the nanostructure sidewall with higher surface energy, i.e. the metal coated surface in this study.

Supporting Information 2 (SI.2)

Uni-directional Wetting on Nanopillars when the Metal Deposition Axis Deviates From the X- or Y-axis

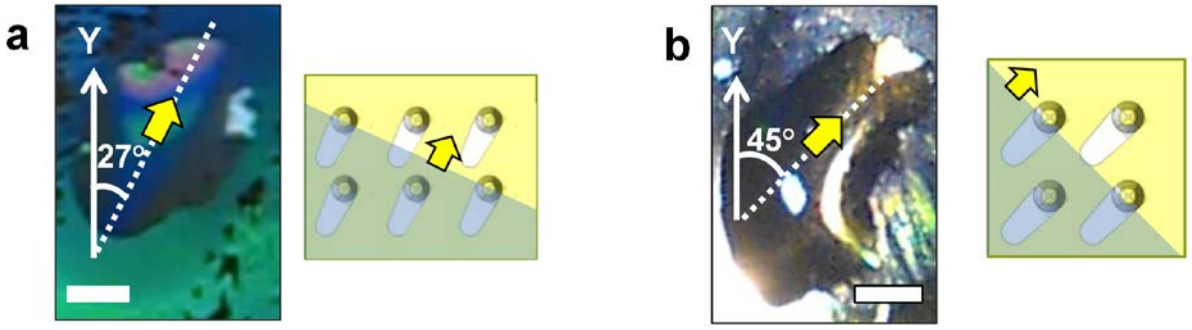

Figure S1: Top views of uni-directional wetting on nanopillars anisotropically coated in the directions (a) β = 207° and (b) β = 225°. Schematic diagram shown beside each picture indicates the movement of the wetting front over the pillars. The yellow arrow indicates the wetting direction which is always opposite to the metal deposition direction and the blue shaded areas on the nanopillar array indicate the wetted regions. Scale bars represent 1mm.

Supporting Information 3 (SI.3)

Derivation of Thermodynamic Equilibrium Apparent Contact Angle, θ_{eqb}, for Droplets on Rough Surfaces with Heterogeneous Surface Chemistry

Table S2a. Symbols used in the derivation of the thermodynamic equilibrium contact angle, θ_{eqb}.

E	Total surface energy of a system comprised of a water droplet and solid surface.
R	Radius of curvature of a droplet on a surface.
H	Height of a droplet on a surface.
A	Radius of the projection of the droplet onto the substrate surface.
A_{app}	Apparent (projected) area of a single repeating unit cell in a nanostructure array. (Example: for a nano-pillar array, A_{app} = (period)^2 = P^2 = $(p+q)^2$ = $(w+v)^2$.
A_{actual}	Actual surface area of a single repeating unit cell in a nanostructure array. (Example: for a nano-pillar array, $A_{actual} = P^2 + \pi ph$.)
R	Roughness defined as A_{actual}/ A_{app}.
S_{ps}	Surface area of PS in a unit cell of a nanostructure array
S_{mtl}	Surface area of metal in a unit cell of a nanostructure array.
γ_{SL}	Surface energy of solid-liquid interface
γ_{SV}	Surface energy of a solid-vapour interface.
γ_{LV}	Surface energy of a liquid-vapour interface.
f_{ps}	Fraction of PS surface area in a unit cell (= S_{ps}/A_{actual}).
f_{mtl}	Fraction of metal surface area in a unit cell (= S_{mtl}/A_{actual}).
V	Volume of droplet.

θ_{eqb}	Apparent water contact angle for a rough surface with chemical heterogeneity at thermodynamic equilibrium.

Starting with a system comprised of a water droplet with the shape of a spherical cap and a substrate surface with both topographical roughness and chemical heterogeneity, the surface energy, *E*, can be written as

$$E = 2\pi RH\gamma_{LV} + \frac{\pi a^2}{A_{app}}\left[S_{ps}\left(\gamma_{SL} - \gamma_{SV}\right)_{ps} + S_{mtl}\left(\gamma_{SL} - \gamma_{SV}\right)_{mtl}\right] \text{---------- (S1)}$$

where R is the radius of curvature of the spherical cap, H is the height of the spherical cap, a is the radius of the circular base of the spherical cap, A_{app} is the apparent (projected) surface area of a unit repeating cell of the nanostructure array, S_J is the actual surface area of material J in that cell (metal or polystyrene in the present case), and γ_{SV}, γ_{SL}, and γ_{LV} are the solid-vapour, solid-liquid and liquid-vapour interfacial energies, respectively.

Knowing that

$$H = R\left(1 - \cos\theta_{eqb}\right), \quad \text{(S2.1)}$$

$$a = R\sin\theta_{eqb}, \quad \text{(S2.2)}$$

$$\frac{S_{ps}}{A_{app}} = \frac{A_{actual}}{A_{app}}\frac{S_{ps}}{A_{actual}} = rf_{ps}, \quad \text{(S2.3)}$$

$$\frac{S_{mtl}}{A_{app}} = \frac{A_{actual}}{A_{app}}\frac{S_{mtl}}{A_{actual}} = rf_{mtl}, \quad \text{(S2.4)}$$

$$\gamma_{LV}\cos\theta_{ps} = \left(\gamma_{SV} - \gamma_{SL}\right)_{ps}, \quad \text{(S2.5)}$$

and

$$\gamma_{LV}\cos\theta_{mtl} = \left(\gamma_{SV} - \gamma_{SL}\right)_{mtl}, \tag{S2.6}$$

the surface energy can be re-written as

$$E = 2\pi R^2\gamma_{LV}\left(1-\cos\theta_{eqb}\right) - \pi R^2\sin^2\theta_{eqb}\, r\gamma_{LV}\left[f_{ps}\cos\theta_{ps} + f_{mtl}\cos\theta_{mtl}\right] \tag{S3}$$

and the volume of the droplet as

$$V = \frac{\pi R^3}{3}\left[\cos^3\theta_{eqb} - 3\cos\theta_{eqb} + 2\right] . \tag{S4}$$

We have determined that the volume of the fluid that is in between the nanostructures in our experiments is insignificant even at water contact angles as low as 3°. For simplicity, it has been neglected in equation (S4).

We can find θ_{eqb} by minimizing E for a fixed V using the method of Lagrange. Taking $\Omega = E + \lambda V$, where λ is a LaGrange multiplier, we find the conditions for which Ω is minimized with respect to both R and θ_{eqb}, giving

$$\frac{d\Omega}{dR} = 4\gamma_{LV} - 2r\gamma_{LV}\left(1+\cos\theta_{eqb}\right)\left[f_{ps}\cos\theta_{ps} + f_{mtl}\cos\theta_{mtl}\right] + \lambda R\left(2+\cos\theta_{eqb}\right)\left(1-\cos\theta_{eqb}\right) = 0 \tag{S5}$$

And

$$\frac{d\Omega}{d\theta_{eqb}} = 2\gamma_{LV} - 2r\gamma_{LV}\cos\theta_{eqb}\left[f_{ps}\cos\theta_{ps} + f_{mtl}\cos\theta_{mtl}\right] + \lambda R\left(1-\cos^2\theta_{eqb}\right) = 0 . \tag{S6}$$

Solving for the equilibrium apparent water contact angle gives

$$\cos\theta_{eqb} = rf_{ps}\cos\theta_{ps} + rf_{mtl}\cos\theta_{mtl} , \tag{S7}$$

where r is the roughness given by $\frac{\text{actual solid-liquid interfacial area}}{\text{projected solid-liquid interfacial area}}$, f_j is the fraction of the solid surface area that is material j and θ_j refers to the intrinsic contact angle of material j given by Young's equation. Equation (S7) can be easily generalized to $\cos\theta_{eqb} = r\sum_{j=1}^{n} f_j\cos\theta_j$ to account for more materials, and can be reduced to the Wenzel[1] and Cassie-Baxter[2] equations under

appropriate assumptions. Note that the droplet is in its lowest energy state when it forms an apparent contact angle of θ_{eqb} with the substrate, i.e. at thermodynamic equilibrium.

Derivation of the Water Contact Angle, θ, Exhibited by Droplets Resting on Nanostructures with Anisotropic Surface Energies

Table S2b. Symbols used to derive the metastable water contact angle, θ, and spreading anisotropy, *S.A.*, used in the characterization of the wetting of droplets on the surfaces.

F_{wet}	Thermodynamic driving force pushing a water droplet to adopt θ_{eqb}.
P	Period of nanostructures normal to the wetting direction.
n	Number of repeating unit cells along the wetting front.
θ	Metastable contact angle observed when a droplet spreads and comes to rest (when $F_{wet} = F_{pin}$) on a textured surface.
F_{pin}	Pinning force, caused by geometric and chemical heterogeneities, preventing the droplet from forming a contact angle of θ_{eqb}.
LVS	Liquid-vapor surface. Essentially the droplet surface that separates the liquid phase and vapor phase.
ϕ_{rest}	The angle of the slope at which an un-relaxed local LVS comes to rest.
ϕ_{pin}	The angle with respect to ϕ_{rest} which the local LVS at the tip of a nanostructure must attain before it can continue to advance to the foot of the nanostructure.
$\phi_{foot\text{-}pin}$	The *additional* angle which the local LVS at the foot of a nanostructure must rotate through before it can continue to advance beyond the foot of the nanostructure. May not exist for certain samples.
l	Pinning length on a single nanostructure.
b	Effective barrier to wetting that takes into account both chemical and structural pinning (=$[l/P][cos\theta_{mtl} - cos\phi_{pin}]$).

S.R.	Spreading ratio.
S.A.	Spreading anisotropy.
L_x	Length of droplet along the axis denoted in the subscript, in this case, *X*.

Derivation of the Wetting Force, F_{wet}

The thermodynamic driving force for wetting at the point when the droplet comes to rest at contact angle, θ, can be easily found by considering the forces acting on the triple phase contact line:

$$F_{wet} = nP(\gamma_{SV} - \gamma_{SL} - \gamma_{LV}\cos\theta) = nP\gamma_{LV}(\cos\theta_{eqb} - \cos\theta)\,, \qquad \text{(S8)}$$

where nP is the projected length of the wetting front, θ is the measured apparent contact angle of the droplet when it comes to rest on a sample and n refers to the number of repeating unit cells with a period of P along the wetting front (Figure S2). The wetting front can be taken as a straight line normal to the direction of wetting and thus P takes the value of $p + q$ for wetting along the *Y*-axis and $w + v$ for wetting along the *X*-axis. While assuming that the contact line is straight seems to contradict what is shown in Figure 5 and Figure 6, it should be noted that the relevant length of the wetting front does not involve the entire triple phase contact line but pertains only to a short section of it at the outermost edge of the droplet, which has been shown through SEM photographs to be straight.[4]

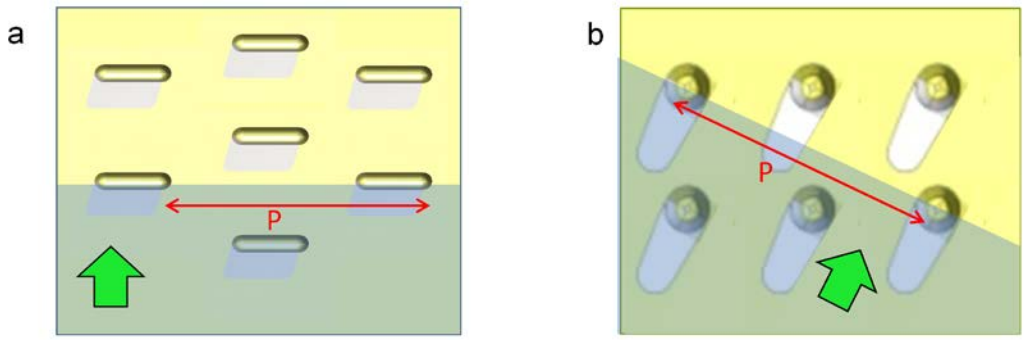

Figure S2: Schematic diagrams showing the period, *P*, for wetting of nanofins along the a) *Y*-axis and b) at an angle of 27° to the Y-axis. The length of the wetting front is essentially equivalent to n repeating units of *P*. Green arrows indicate wetting directions and are normal to *P*.

Although F_{wet} will only vanish when $\theta = \theta_{eqb}$, droplets spreading on rough surfaces rarely come to rest at θ_{eqb} as motion of the wetting front can be easily arrested by protrusions, cavities and chemical heterogeneities which trap the triple phase contact line and constrain the system in a metastable state[3] in which the pinning force of the nano-defects, F_{pin}, balances F_{wet}. In other words, the droplet does not come to rest at thermodynamic equilibrium, for which $F_{wet} = 0$, but at a metastable state for which $F_{wet} = F_{pin}$. As a result, droplets in experiments will exhibit a static apparent contact angle of θ which is greater than θ_{eqb} since F_{wet} is greater than zero.

Derivation of the Pinning Force, F_{pin}, and θ

To compute θ, F_{pin}, which adopts a form similar to that of Equation (S8), has to be expressed in terms of the pinning length and pinning angle. Both of these values can be estimated from the geometry of the nanostructures. With reference to Figure S3a, consider first the approach of the liquid-vapor surface (LVS) toward a nanostructure in the direction of the metal coated face.

As the LVS advances across the PS floor to the left of the nanostructure, it translates with a local contact angle equivalent to the intrinsic angle of the PS, θ_{ps}. This intrinsic angle is determined by the local surface energies and is different from the macroscopic apparent angle which is a result of spatially averaged surface energies. When the LVS reaches the nanostructure, it scales the side of the structure with essentially the same contact angle, θ_{ps}, with respect to the

horizontal. Movement of the LVS up the nanostructure does not prove to be a problem as the local contact angle is greater than θ_{ps} and the net force on the LVS brings it upward. At the top of the nanostructure, however, the LVS will attempt to relax from θ_{ps} to θ_{mtl} as the material at the top is the metal coating and not PS. As can be observed in Figure S3b, when the LVS forms a local contact angle of θ_{ps} with the metal coating at the top of the nanostructure, there is a net force of $\gamma_{SV,mtl} - \gamma_{SL,mtl} - \gamma_{LV}cos\theta_{ps} = \gamma_{LV}cos\theta_{mtl} - \gamma_{LV}cos\theta_{ps}$ per unit length acting on the triple phase contact line, pulling it to the right. As the triple phase contact line advances, the local contact angle the LVS makes with the metal coating decreases until it reaches θ_{mtl}. The triple phase contact line then comes to rest when the local surface forces are balanced. In Figure S3b, it can be seen that this relaxation will take place entirely on the horizontal portion at the top of the nanostructure if the width of the nanostructure (parallel to the wetting direction) is wide enough to accommodate the process. Here, we assume that the minimum width of a nanostructure that will allow for this is approximately 1-10μm, which is the size of the local LVS.[4]

If the width of a nanostructure is *small* compared to the size of the local LVS (≤0.2μm), the LVS will not have enough room to relax from θ_{ps} to θ_{mtl} on the horizontal portion of the top of the nanostructure. As a result, the force acting on the triple phase contact line will bring the LVS to the rounded edge of the nanostructure beyond the horizontal portion, and equilibrium for the local surface tensions γ_{SV}, γ_{SL} and γ_{LV} is achieved at a slope of ϕ_{rest} where the LVS makes a local contact angle of θ_{mtl} with the tangent to the curvature (Figure S3c). Since the width of the nanostructure is narrow, we assume that there is almost no relaxation of the LVS on the horizontal portion of the top of the nanostructure i.e. $\phi_{rest} + \theta_{mtl} = \theta_{ps}$ (Figure S3c).

Note that the relaxation of the local contact angle from θ_{ps} to θ_{mtl} on the top of the nanostructure will be spontaneous even in the absence of an external force. This relaxation ends

with the LVS attaining a contact angle of θ_{mtl} with respect to the surface, which may be horizontal or slanted. This is therefore, the "resting" state of the LVS and thus, all subsequent rotations of the LVS caused by F_{wet} have to be measured relative to the surface at this "resting" state.

For the LVS to move down the right slope of the nanostructure, an angle of $\alpha + \theta_{mtl}$ with respect to the horizontal is required,[4] and the pinning strength required at the top of the nanostructure is the force that is required to rotate the blue LVS to the red LVS in Figure S3d. This essentially means that the LVS has to turn from a local contact angle of θ_{mtl} to $\phi_{pin} = \alpha - \phi_{rest} + \theta_{mtl}$ (measured relative to the red dashed line in Figure S3d which represents the surface at the "resting" state) to advance down the side of the nanostructure. After this, the LVS relaxes from $\alpha + \theta_{mtl}$ to θ_{ps} on the floor to the right of the nanostructure in Figure S3a, and the process repeats until the driving force for wetting can no longer overcome the contact line pinning caused by the nanostructure. Hence, the maximum pinning force on the wetting front can now be expressed as

$$F_{pin} = nl\gamma_{LV}\left(\cos\theta_{mtl} - \cos\phi_{pin}\right), \tag{S9}$$

where nl is the length of the wetting front that is pinned and l is the pinning length provided by a single nanostructure. Finally, equating Equations (S8) and (S9) gives Equation 1.

We have assumed that viscous dissipation will eliminate any excess energy of the droplet before it reaches the metastable state. Therefore, when $F_{wet} = F_{pin}$, the wetting front will come to a halt instead of moving on with constant velocity, i.e. no excess energy is carried forward to help the wetting front surmount the energy barrier. This assumption is based on the observation that the triple phase contact line tends to move in a stick-slip manner as the droplet is coming to rest, often "jumping" from one surface asperity to another.[5]

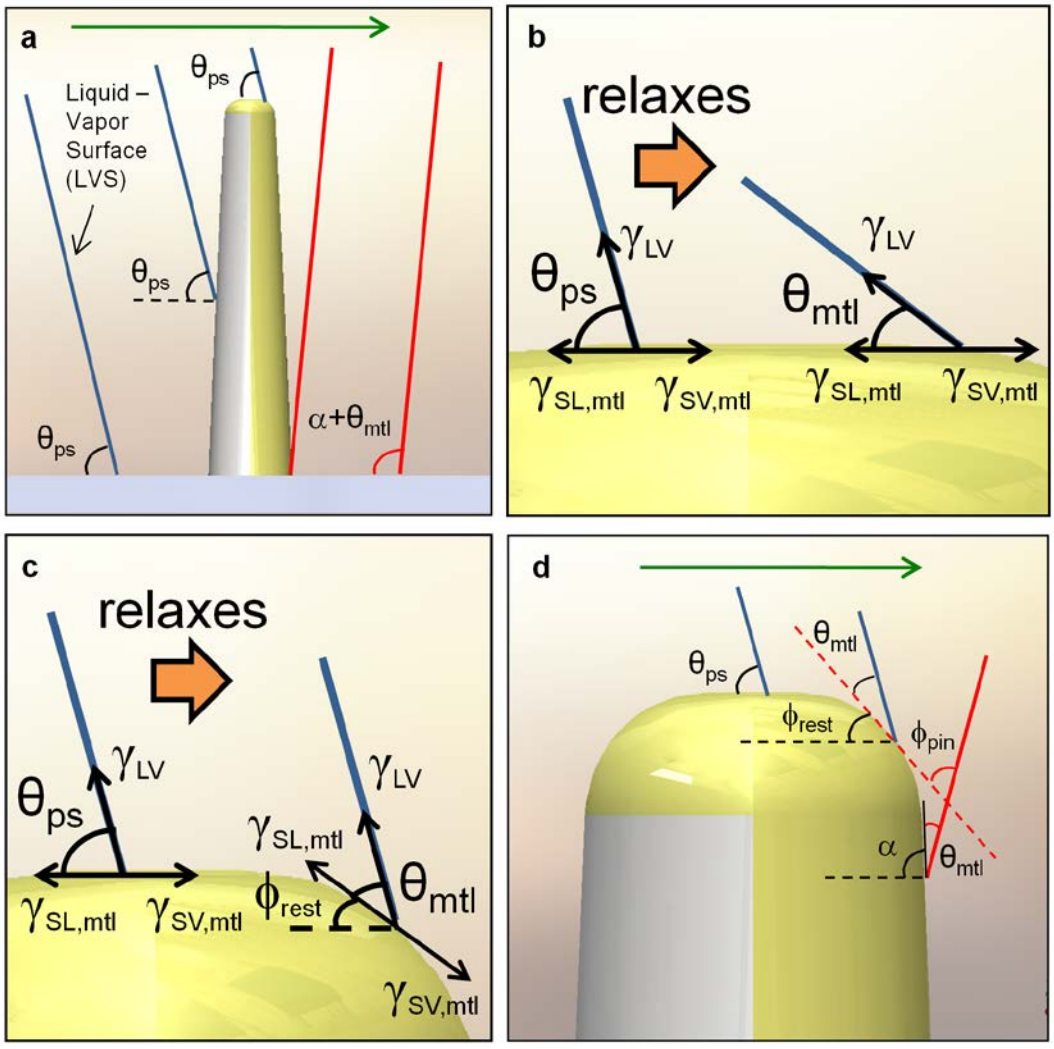

Figure. S3 (a) Schematic diagram showing the various positions of the LVS as it moves past a nanostructure from left to right. (b) Magnified view showing the relaxation of the LVS from θ_{ps} to θ_{mtl} on a nanostructure with a wide tip. (c) Magnified view showing the relaxation of the LVS from θ_{ps} to θ_{mtl} on a nanostructure with a narrow tip. (d) Magnified view showing the pinning of the LVS at the top of the nanostructure. Note that the area to the left of a LVS is filled with liquid whereas the area to the right of a LVS is not. Blue and red lines represent positions of the LVS before and after overcoming the pinning at the nanostructure, respectively. Green arrow indicates the direction of wetting.

Additional Considerations for Wetting over a Hydrophobic Floor and Wetting in the Direction of the Uncoated Face

Additional constraints have to be accounted for in the cases where the LVS moves over hydrophobic floor materials and when it travels in the direction of the uncoated face. For hydrophobic materials, for which $\theta_{ps} > 180^{o}-\alpha$, a physical constraint is imposed on the LVS such that it can only scale the left slope of the nanostructure at an angle of $180^{o}- \alpha$, which corresponds to a maximum local contact angle of 180^{o} (Figure S4a). As a result, the contact angle with respect to horizontal at the top of the nanostructure for this case is $180^{o}- \alpha$ instead of θ_{ps}. In addition, after the LVS has reached the bottom of the nanostructure, it may be required to rotate through an additional $\phi_{foot\text{-}pin}$ to θ_{ps} before it can advance further on the PS floor on the right (Figure S4a) (See Worked Example below). Thus, the LVS has to rotate to a final contact angle of $\phi_{pin} + \phi_{foot\text{-}pin}$ (measured relative to the "resting" state) before it can advance past a nanostructure.

Next we consider wetting in the direction of the uncoated face. A special scenario may arise where the LVS may be trapped at the transition between the metal and PS (assuming the change of material is abrupt) at a slope of $90^{o}– \delta$ with a local contact angle greater than θ_{mtl} (Figure S4b). This happens when $\phi_{rest} = [(180°-\alpha) - \theta_{mtl}] > (90^{o}– \delta)$ i.e. the LVS has not reached the gradient of ϕ_{rest} where the local contact angle can fully relax to θ_{mtl} before its advance is halted by a sudden transition from metal to the more hydrophobic PS. The local contact angle the LVS makes with the tangent to the edge at this new "resting" point is $180°-\alpha-90°+\delta = 90°-\alpha+\delta$ instead of θ_{mtl} at a slope of $90^{o}– \delta$ instead of ϕ_{rest}. The appropriate substitutions will then have to be made in the computation described earlier. Note that this need not always be the case. As shown in Figure 4c, if δ is small enough, the LVS can reach a local contact angle of θ_{mtl} at a

slope of ϕ_{rest} before or at the transition point from metal to PS. In this case, the analysis is similar to that of wetting in the direction of the metal coated face (Figure S3).

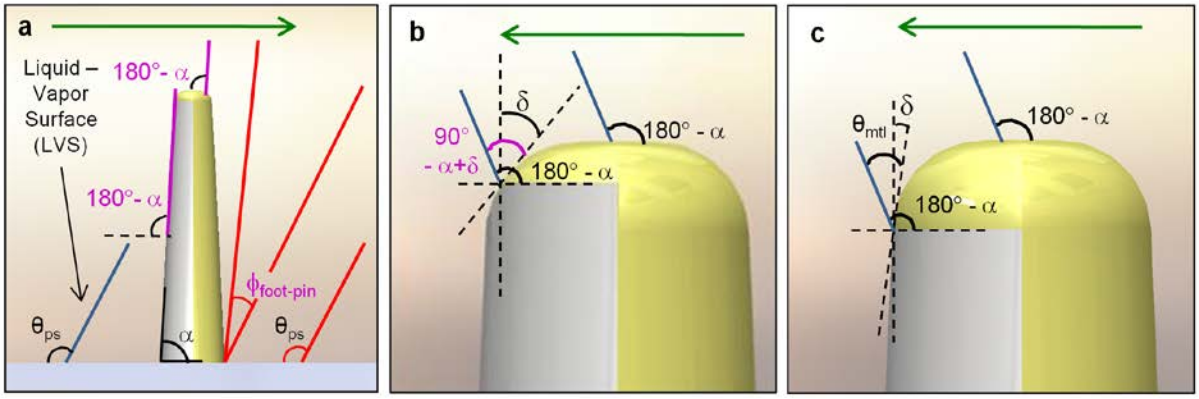

Figure S4. Schematic diagrams showing the movement of the LVS over a nanostructure. (a) Nanostructure with hydrophobic floor (b) Magnified view showing the LVS pinned at the transition from metal to PS with a local contact angle greater than θ_{mtl} when wetting in the direction of the uncoated face. (c) Magnified view showing the LVS unaffected by the transition from metal to PS as it is able to reach the slope ϕ_{rest}, which is before or at the transition point at which it can relax to form a local contact angle of θ_{mtl}. Purple lines and font highlight modified parameters. Green arrows indicate the directions of wetting.

Reduction of the Pinning Length, l, due to Curvature of the Nanostructures

Careful attention must also be paid in the estimation l in Equation (S9), which, in this model, requires a rigorous approach that takes the curvature of the nanostructures into account. The modification of l due to the contours of the nanostructures will prove to be significant for nanopillars and the faces of nanofins parallel to the *Y*-axis, but not so much for the faces of the nanofins parallel to the *X*-axis. Based on simulations done by Forsberg *et al*,[5] it was found that pinning of the triple phase contact line on surface protrusions occurs differently for materials

with different wettability. In the case in which the front face and floor material are as hydrophilic as Al and Ni, the liquid will wet the nanostructure from the bottom up, leaving only the triple phase contact line at the top of the nanostructure pinned. For this reason, we will focus only on the pinning force, and therefore the pinning length, provided by the top of the nanostructures.

Figure S5 shows schematic diagrams for the movement of the wetting front over a nanostructure. In Figure S5a, it can be seen that the top of the nanopillar is effectively a truncated spherical cap that causes a reduction of l as the wetting front passes over the nanostructure as demonstrated in Figure S5b. In addition, because of the spherical nature of the edge, the local contact angle is the same everywhere along the triple phase contact line at the edge at any given instance, no matter if it is viewed from the side (Figure S5c) or the top (Figure S5d). The black lines represent the LVS when it is "resting" at the edge of the nano-pillar at a slope ϕ_{rest} with respect to the horizontal. In the presence of F_{wet}, the contact angle increases until the wetting front reaches the red lines in Figure S5c and Figure S5d, at which point the fluid overcomes the pinning force at the top and moves down the pillar. At this point, the angle the LVS makes with the horizontal in Figure S5c and Figure S5d is $\alpha + \theta_{mtl}$ and it can be shown from simple geometry that $\phi_r = \alpha$. Thus, l can be computed to be $w\cos\alpha$.

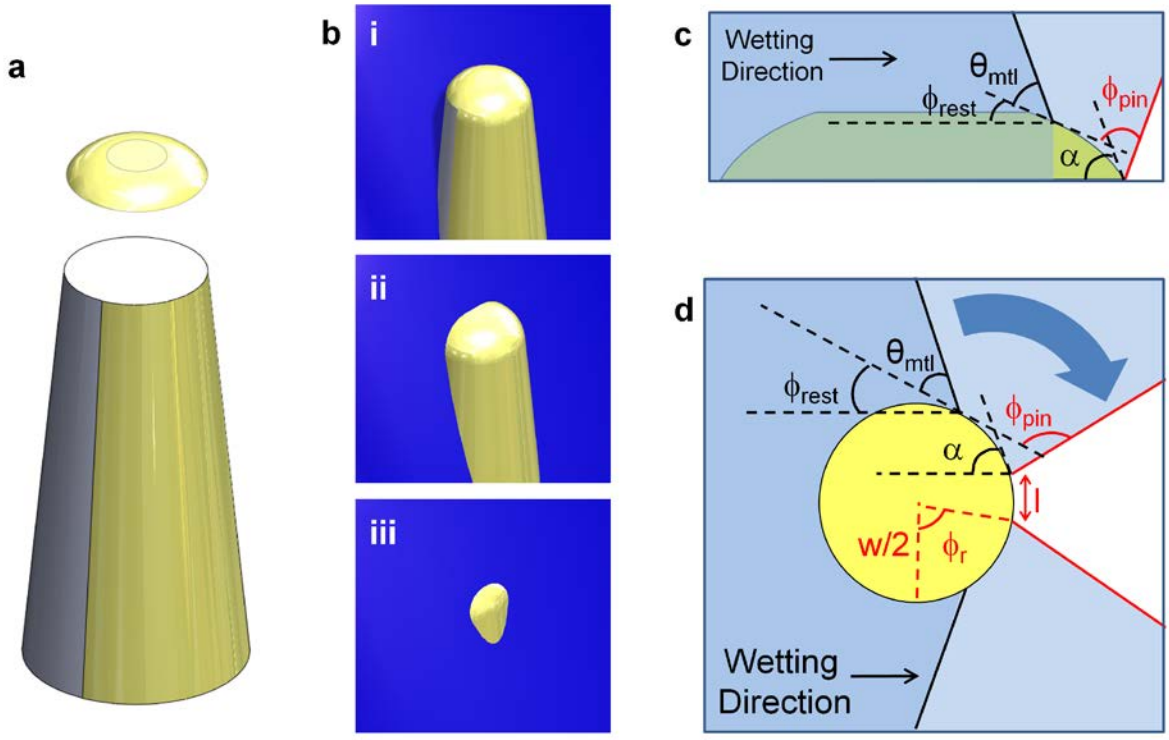

Figure S5. (a) Schematic diagram showing a nanopillar modelled as a tapered rod with a truncated spherical cap as a tip. (b) Schematic illustration showing the reduction of the pinning length at the tip as the wetting front advances across a nanopillar. (c) Side view of the process in (b). Black lines represent the resting position of the wetting front and red lines represent the critical point when the pinning force at the tip is overcome and the liquid is allowed to travel down the nanopillar. (d) Top view of the process in (b). The dark blue arrow indicates the direction of rotation of the wetting front from the black lines to the red lines.

Worked Examples

As an illustration of the use of Equation (1), consider the worked example for hydrophobic nanofins for which β = 180° (sample H). From Equation (S7),

$$\cos\theta_{eqb} = rf_{ps}\cos\theta_{ps} + rf_{mtl}\cos\theta_{mtl},$$

which can be written in terms of the surface areas of the metal coated and uncoated regions in a single cell:

$$\cos\theta_{eqb} = \frac{S_{mtl}\cos\theta_{mtl} + S_{ps}\cos\theta_{ps}}{A_{app}}.$$

Using the appropriate geometric parameters (Figure S6) to calculate the surface areas of metal-coated and uncoated regions in a single cell,

$$\cos\theta_{eqb} = \frac{\left[ph + \frac{(q-p)}{2}(w+v) + pw + 2wh\right]\cos\theta_{mtl} + (ph + pv)\cos\theta_{ps}}{(w+v)\left(p + \frac{q-p}{2}\right)}$$

$$\theta_{eqb} = 41.59°$$

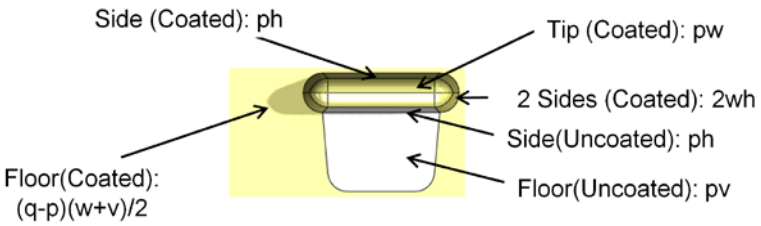

Figure S6. A unit cell of nanofin.

From Equation (1),

$$\cos\theta = \cos\theta_{eqb} - \frac{l}{P}\left(\cos\theta_{mtl} - \cos\phi_{pin}\right),$$

and so, in the direction of the metal coated face which is aligned with $+Y$ in this particular case,

$$\cos\theta = \cos\theta_{eqb} - \left[\frac{p}{p+q}\right]\left[\cos\theta_{mtl} - \cos\left(\phi_{pin} + \phi_{foot-pin}\right)\right]$$

Since θ_{ps} = 115° > (180°- α), contact angle at the top of the nanostructure is (180°-α) = 180°-85° = 95˚and ϕ_{rest} = 95° - θ_{mtl} = 95° - 22° = 73°. To move down the right-side slope, an angle of α +

θ_{mtl} = 107° with respect to the horizontal is required. Hence, ϕ_{pin} = 107° - 73° = 34°. To move beyond the foot of the nanostructure, an angle of 115° (θ_{ps}) is needed. Therefore, the LVS requires an additional rotation of $\phi_{foot\text{-}pin}$ = 115° -107° = 8°. The final angle that the LVS has to rotate to move past the nanostructure is ϕ_{pin} + $\phi_{foot\text{-}pin}$ = 42° with respect to the tangent to the edge at ϕ_{rest}. From this, θ_{+Y} is found to be <u>48.4°</u>.

As for wetting in the direction of the uncoated face which is aligned with –*Y*, here

$$\cos\theta = \cos\theta_{eqb} - \left[\frac{p}{p+q}\right]\left[\cos(90° - \alpha + \delta) - \cos\phi_{pin}\right].$$

Similar to the analysis above, the contact angle at the top of the nanostructure is (180°-α) = 95°, since the LVS also passes along the hydrophobic PS floor before scaling and reaching the tip of the nanostructure when travelling to the left in Figure S4b. At the edge of the structure, Al transits to PS at an angle of 90°- δ = 63° to the horizontal. The LVS is thus trapped at the transition point at an angle of 90°-α+δ = 90°-85°+27° = 32° (>θ_{mtl}). Since the LVS has to turn from a local resting angle of 90°-α+δ to ϕ_{pin} instead of θ_{mtl} to ϕ_{pin}, (cosθ_{mtl} - cosϕ_{pin}) of equation (1) is substituted with [cos(90°-α+δ) - cosϕ_{pin}] for this case. To move down the left-side slope, an angle of α+θ_{ps} = 85° + 115° = 200° with respect to the horizontal is required. Therefore, ϕ_{pin} = 200° - 63° = 137° (as seen from ϕ_{rest}). There is no $\phi_{foot\text{-}pin}$ because the LVS will contact the PS floor on the left side with a local contact angle of 180°. The final angle that the LVS has to reach to move past the nanostructure is then ϕ_{pin} =137°. θ_{-Y} is found to be <u>88.6°</u>.

For the *X*-axis, where the nanostructures have isotropic surface energy,

$$\cos\theta = \cos\theta_{eqb} - \left[\frac{w\cos\alpha}{w+v}\right]\left(\cos\theta_{mtl} - \cos\phi_{pin}\right).$$

Because p = 3.33μm, we consider the LVS to have fully relaxed at the tip of the nano-fin when moving along the *X*-axis. Hence, the contact angle at the top of the nanostructure is θ_{mtl} = 22° and ϕ_{rest} = 0°. To move down the slope, an angle of $\alpha + \theta_{mtl}$ = 85° + 22° = 107° with respect to the horizontal is necessary. The LVS will contact and move across Al at the foot of the nano-fin along the X-axis, and since 107°>θ_{mtl}, there is no pinning at the foot. Because w is small, the radius of curvature now plays a significant role and $l = w\cos\alpha$. θ_X is found to be 43.0°. As a comparison, the experimental values are $\theta_Y = \theta_{+Y}$ = 51.5° ± 1.1° and θ_X = 42.4° ± 6.2°.

References

1. Wenzel, R. N. Resistance of solid surfaces to wetting by water. *Ind. Eng. Chem.* **1936**, *28*, 988–994.
2. Cassie, A. B. D.; Baxter, S. Wettability of porous surfaces. *T. Faraday Soc.* **1944**, *40*, 546-551.
3. Johnson, R. E. & Dettre, R. H. Contact Angle Hysteresis I. Study of an Idealized Rough Surface. *Contact Angle, Wettability and Adhesion* **1964**, *43*, 112–135.
4. Choi, W.; Tuteja, A.; Mabry, J. M.; Cohen, R. E.; McKinley, G. H. A modified Cassie-Baxter relationship to explain contact angle hysteresis and anisotropy on non-wetting textured surfaces. *J. Colloid Interf. Sci.* **2009**, *339*, 208–216.
5. Forsberg, P. S. H.; Priest, C.; Brinkmann, M.; Sedev, R.; Ralston, J. Contact Line Pinning on Microstructured Surfaces for Liquids in the Wenzel State. *Langmuir* **2010**, *26*, 860–865.